CrystEngComm

Accepted Manuscript

ROYAL SOCIETY OF CHEMISTRY

www.rsc.org/crystengcomm

Journal Name

ARTICLE

Fabrication of CdS/BNNSs nanocomposites with broadband solar absorption for efficient photocatalytic hydrogen evolution

Received 00th January 20xx,
Accepted 00th January 20xx

DOI: 10.1039/x0xx00000x

www.rsc.org/

Fukun Ma, Gang Zhao, Chen Li, Tailin Wang, Yongzhong Wu*, Jiaxin Lv, Yueyao Zhong, Xiaopeng Hao*

In this work, the nanocomposites of cadmium sulfide (CdS) nanoparticles and hexagonal boron nitride nanosheets (BNNSs) were fabricated through in-situ growing of CdS nanoparticles on BNNSs. The microstructure of the nanocomposites was demonstrated clearly. Compared with pure CdS nanoparticles, CdS/BNNSs nanocomposites show more efficient on photocatalytic H_2 production. The rate of H_2 evolution can be increased twice more under the optimum conditions. The enhancement of photocatalytic H_2 evolution is attributed to the ultrathin BNNSs. It is speculated that the BNNSs not only broaden the photo absorption region, but also realized the effective electronic communication through the connection between CdS nanoparticles and BNNSs. This new finding provides a promising way to design and fabricate more efficient photocatalysts based on BNNSs.

1. Introduction

Due to the two-dimensional layer structure analogous to graphene,[1-3] hexagonal boron nitride nanosheets (BNNSs) have received a great deal of attention for potential applications from both the experimental and theoretical science communities since graphene has attracted enormous interest.[4-7] Up to now, many elaboration works have been devoted to the properties and potential application of BNNSs such as electrical resistance,[8-9] thermal conductivity,[10-11] catalytic activity,[12-13] and optoelectronic properties.[14-15] In addition, the BNNSs supporters can be appealing candidates because they provide a platform for attaching the particles and endowing the "defective" particle surface with high active sites.[16] So the impact of BNNSs in association with other nanomaterials to produce nanocomposites with promising potential applications such as sensors, energy storage, and catalysis has captured the interest of some researchers.[17-20] For example, BNNSs supported on Au was theoretically suggested and experimentally proved to act as an electrocatalyst for oxygen reduction reaction.[21]

However for photocatalytic activity, in common BNNSs are considered to have no effect, since h-BN is an insulator with a wide band gap (3.6−7.1 eV depending on experimental methods).[22-23] But to our surprise and excitement, BNNSs show unique properties compared with bulk h-BN. Firstly, the band gap of the BNNSs can be significantly reduced by B- and N-vacancies and impurity defects.[16, 24] Secondly, the atomically thin h-BN nanoribbons are shown to possess semiconducting properties due to conducting edge states and vacancy defects.[16] Thirdly, electron tunneling through ultrathin h-BN layers deposited on a gold surface was demonstrated.[25] Therefore, it seems to be fulfilled that ultrathin BNNSs may play a crucial role in the respect of improving the performance of photocatalysis materials.

CdS is one of the most vital and classical chalcogenide semiconductors, and its narrow but direct bandgap (2.4 eV) is effective for capturing the visible light and water splitting.[26-28] However, the overquick radiative recombination of photogenerated electrons and holes in solar activated CdS and the high kinetic barrier for hydrogen production over its surface sites do not allow the direct conversion of solar energy to hydrogen gas.[29-31] Meanwhile, CdS shows a relatively limited spectral response range, only light with enough photon energy (shorter than 510 nm) is able to be absorbed.[32-33]

Here the nanocomposites of CdS nanoparticles and BNNSs with broad spectral response were designed and fabricated for efficient hydrogen production from water. For the first time, the CdS nanoparticles were shown to grow in-situ on the BNNSs. And because of the feature of broad spectral response, the new nanocomposites showed efficient photocatalytic performance. According to this result, BNNSs augur well for the broader prospects in the electron conduction and photocatalysis field.

2. Experimental

2.1 Preparation of BNNSs.

Dr. F. K. Ma, G. Zhao, C. Li, T. L. Wang, J. X. Lv, Y. Y. Zhong, Prof. Y. Z. Wu, Prof. X. P. Hao
State Key Lab of Crystal Materials, Shandong University, Jinan, 250100, China.
E-mail: xphao@sdu.edu.cn

Electronic Supplementary Information (ESI) available: Experimental section and supplementary figures. See DOI: 10.1039/x0xx00000x

In a typical experiment, 10 mol/L sodium hydroxide aqueous solution was prepared as dispersing agent. And then 30 mL dispersing agent was put into a clean flask containing 0.2 g h-BN powder. After that, the flask was capped and bath-sonicated for 24 h. The flask was taken out and a slight odor of ammonia was noticed when the vial was opened. The product was collected and washed with deionized water repeatedly until the pH of the filtrate was close to neutral. The product was placed in a 500 mL beaker with almost a full glass of ethanol, after the beaker was shaken for several times, the dispersion was allowed to settle for two weeks to sediment out these undispersed particles as much as possible. Then the supernatant was collected and about 20 mg BNNSs from 0.2 g bulk BN were obtained for further use.

2.2 Synthesis of CdS/BNNSs nanocomposites.

Several certain weight BNNSs were dissolved in 30 mL ethanediol. Then 0.343 g $Cd(SCN)_2$ and 0.285 mL [BMIM]SCN were also added to the ethanediol. The ethanediol solvents were added to poly-(tetrafluoroethylene)-lined autoclaves of a microwave digestion system after all the reagents were dissolved. The autoclaves were maintained at 180 °C for 30 min. After cooling down to room temperature, the precipitation was filtered and washed with ethanol and water several times. At last, almost the same weight of 0.1960 g CdS/BNNSs nanocomposites with certain weight BNNSs (0, 0.1, 0.5, 1, 1.5 wt%) were got following by the vacuum-dried at 40 °C.

2.3 Characterization.

Scanning electron microscopy (SEM) was performed on a Hitachi S-4800 field emission scanning electron microscope. High-resolution transmission electron microscopy (HRTEM) images were obtained with a Philips Tecnai 20U-Twin high-resolution transmission electron microscope at an acceleration voltage of 200 kV. The X-ray photoelectron spectroscopy (XPS) was performed on an ESCALAB 2200-XL X-ray photoelectron spectrometer. X-ray powder diffraction (XRD) patterns were obtained on a Bruker D8 advance X-ray diffractometer with Cu-Kα radiation (λ = 0.15418 nm). Absorption spectra were taken on a Hitachi U-3500 UV-vis spectrometer.

2.4 Hydrogen evolution reaction (HER) measurements.

Photocatalytic reactions were carried out in a Pyrex reaction cell connected to a closed gas circulation and evacuation system. The optimised photochemical reaction continued throughout the HER process. In brief, 50 mg of nanocomposites were dispersed in 100 mL of aqueous solution containing 0.7564 g Na_2S and 4.8036 g Na_2SO_3 as sacrificing agents. The suspension was then thoroughly degassed and irradiated by a Xe lamp (300 W). The temperature of the reactant solution was maintained at 5 °C by flowing cooling water during the reaction. The amount of H_2 produced was analysed using an online gas chromatography. The activities of the nanocomposites were compared using the average rate of H_2 evolution every 5 h.

The photocatalytic quantum efficiency (QE) for H_2 evolution was measured using a typical experimental setup. The nanocomposites solution was irradiated with a 300 W Xe lamp by applying a band-pass filter (420 nm) for 5 h. The average intensity of irradiation was determined by a PL-MW2000 optical power meter (Beijing Perfect light Technology Ltd, China), and the irradiation area is 18.85 cm^2. Hence, QE can be estimated as follows:

$$QE = \frac{2\times\text{the number of evolved } H_2 \text{ molecules}}{\text{the number of incident photons}}$$

2.5 Photoelectrochemical activity measurements

Photoelectrochemical test systems contained a CHI660D workstation (Shanghai Chenhua, China) with a three-electrode configuration using the prepared samples as the working electrodes, a Pt plate as the counter electrode, Ag/AgCl as the reference electrode and a 300 W Xe lamp equipped as the light source. Na_2SO_4 aqueous solution (0.5 M) with 20% lactic acid was used as the electrolyte. The working electrodes were prepared as follows: 10 mg of the as-prepared nanocomposites (0.5 wt%) were dispersed in absolute ethanol, and the suspension was directly deposited onto an indium-tin oxide (ITO) glass plate and then dried at 80 °C in a vacuum oven. Electrochemical impedance measurements were performed within a frequency range of 0.1 kHz to 100 kHz.

3. Results and discussion

3.1 Structure, morphology and chemical composition characterization.

Firstly, scanning electron microscopy (SEM) was used to probe the morphologies of the as-prepared CdS/BNNSs nanocomposites (Fig. 1). Fig. 1a showed the exfoliated BNNSs. From the SEM image, the BNNSs were almost entirely transparent even at a lower accelerating voltage, which demonstrated the ultrathin nature of BNNSs.[34] Fig. 1b showed the pure CdS which had a spherical structural with an average diameter of about 50 nm. CdS/BNNSs nanocomposites can be seen in Fig. 1c, d. From the images, the CdS nanostructures were found to grow on the edges and asperities of BNNSs. So, the formation mechanism of the nanocomposites can be understood in terms of the kinetic process of heterogeneous nucleation theory. The growth process of CdS nanoparticles on BNNSs belongs to heterogeneous nucleation and the surfaces of BNNSs, especially the vacancy defects, serve as low energy barrier centre for the nucleation of new phases.[35] In this case, CdS nanoparticles were grown as solid droplets on the surfaces of BNNSs.

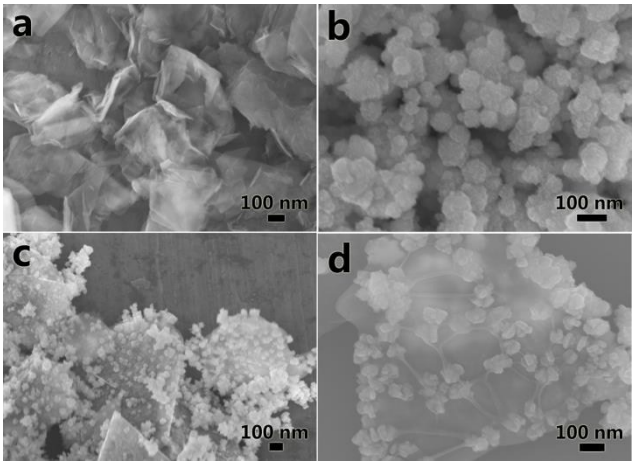

Fig. 1 SEM images of BNNSs (a), CdS nanoparticles (b) and CdS/BNNSs nanocomposites (c, d).

Further crystal characterizations for the CdS/BNNSs nanocomposites were shown in Fig. 2 using the HRTEM images. Fig. 2a showed a single BNNS covered by lots of CdS nanoparticles. It can be seen clearly that the CdS nanoparticles was grown on the edges and asperities of BNNS which was consistent with the SEM images. Fig. 2b showed the lattice structure of a part of CdS nanoparticles which grown on the edges of BNNSs. The obvious crystalline interplanar spacing on the picture was figured out as 0.334 nm which shows the (002) of CdS. Meanwhile the pattern revealed the BNNSs lattice structure. From this picture the lattice of BNNS can be observed distinctly, it showed the BNNSs kept well-crystallized after the exfoliation process. And the distance between the two neighboring bright reflections in the inset of Fig. 2b was 0.258 nm which was perfectly corresponds to the B-B or N-N atom separations in BNNSs. The electron diffraction pattern of CdS/BNNSs nanocomposites was shown as an inset. Since the electron diffraction pattern of CdS polycrystalline structure was annulus, and the pattern of BNNSs was hexagonal lattice, the image of CdS/BNNSs electron diffraction pattern can be shown as the superposition of the two patterns. From these images, it was proved directly in another way that CdS nanoparticles were in-situ grown on BNNSs and combined together closely.

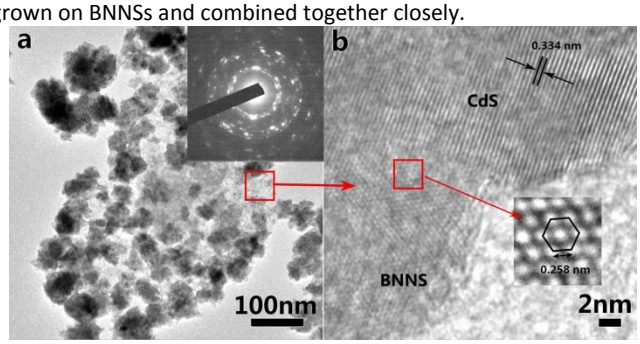

Fig. 2 TEM images of 0.5 wt% CdS/BNNSs. (a) A single BNNS covered by CdS nanoparticles; The inset showed the electron diffraction pattern of CdS/BNNSs nanocomposites. (b) The lattice structure of CdS nanoparticles and BNNS.

XPS is a particularly useful tool to study the composition and electronic structure of materials. A survey XPS spectrum in Fig. 3a exhibited the detailed peaks of CdS/BNNSs nanocomposites, including O 2s, S 2p, S 2s, C 1s, N 1s, B 1s, and Cd 3d. The peaks of O and C were mainly caused by the silica substrate and surface contamination. As shown in Fig. 3b, a typical high resolution XPS spectrum of Cd 3d was presented. Two peaks at 405.0 and 411.9 eV were assigned to Cd 3 $d_{5/2}$ and 3 $d_{3/2}$, which were characteristic peaks of Cd^{2+} in CdS nanoparticles. As for the high resolution spectrum of N 1s (Fig. 3c), the small peak at 397.7 eV was attributed to N 1s. This peak was not obvious because of the low amount of BNNSs (about 0.5 wt%) in the nanocomposites, which was the same as the peak of B 1s in Fig. 3d. [36] The XPS spectrum of the B 1s region can be fitted into two peaks: 190.7 eV and 191.6 eV, which were corresponding to B-N and B-O, respectively (Fig. 3d).[37] Fig. 3e showed the XPS spectrum of the S 2p region, which can be fitted into two peaks: 162.7 eV and 164.0 eV. The peak of 162.7 eV was corresponding to the S^{2-} in CdS nanoparticles, [38-39] and the appearance of the peak at 164.0 eV can be speculated to the new chemical bond during the in-situ growth progress. And since the binding energy of S 2p shift higher slightly, the formation of S-O bond is predicted. The XPS results further confirm the coexistence of BNNSs and CdS nanoparticles in the nanocomposites. The slight shift of S 2d and B 1s shows the presumable presence of B-O-S chemical bonds between CdS and BNNSs. These new chemical bonds may have contributed to the broader spectral response range and effective electronic communication between BNNSs and CdS.

Journal Name

ARTICLE

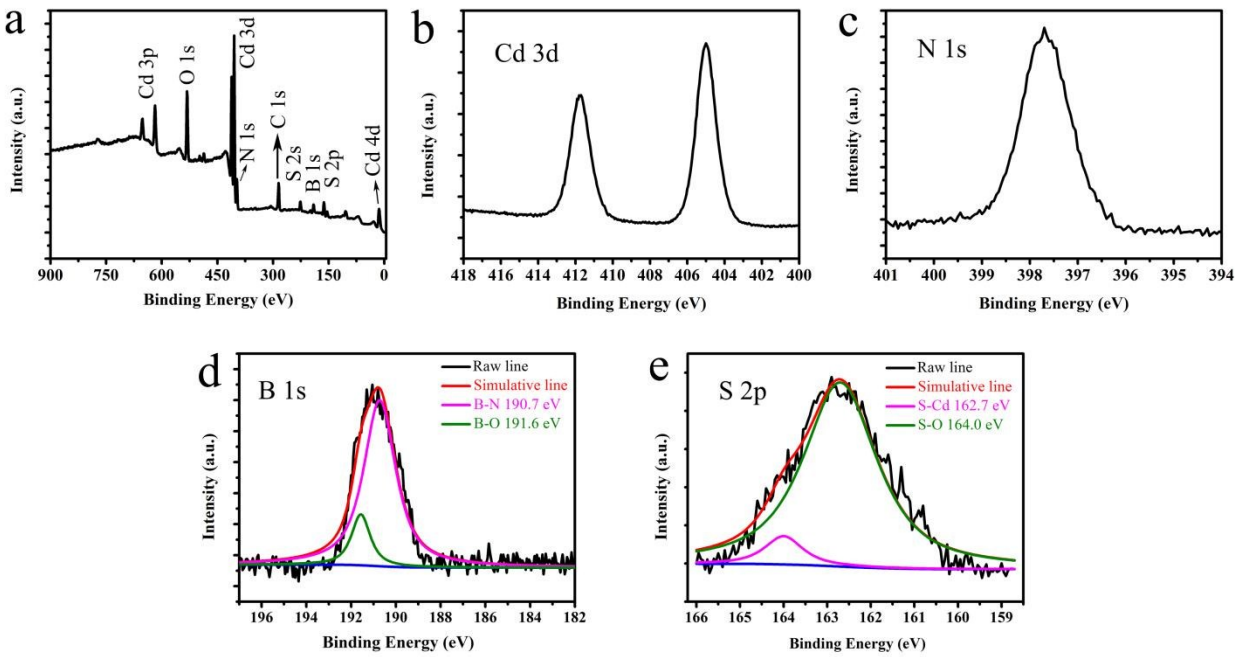

Fig. 3 XPS spectra for CdS/BNNSs nanocomposites (0.5 wt%). a) A survey spectrum of CdS/BNNSs nanocomposites. b) High resolution XPS of the Cd 3d region. c) The N 1s region. d) The B 1s region. e) The S 2p region.

Furthermore, the crystal structure of the as-obtained products was investigated by XRD. Fig. 4 showed the XRD patterns of these products. The above two patterns and showed the XRD of BNNSs and pristine h-BN powder. These two lines showed the diffraction peaks of the as-prepared BNNSs and pristine BN powder corresponding to the (002), (100) and (004) planes of the hexagonal BN, respectively, with lattice constants of a = 0.2504 nm and c = 0.6656 nm (JCPDS card 34-0421). It should be noticed that no impurities were detected in the first blue line, which indicated the as-prepared BNNSs were pure. Moreover, it was interesting to note that the peaks of BNNSs became weaker than that of pristine BN powder and the other diffractions such as (110) and (102) almost disappeared, which led one to speculate that the (002) and (004) crystal faces of BNNSs were exposed, and the BNNSs were exfoliated from the precursor BN powder along the (002) plane without destroying its crystalline structure.[40] The bottom black line was the pure CdS nanoparticles, the diffraction peaks were well indexed to crystal planes of a hexagonal phase CdS (JCPDS no. 41-1049). What's more, the diffraction peaks of the CdS/BNNSs nanocomposites (0.5 wt% and 10 wt%) were also well indexed to the crystal planes of hexagonal phase CdS. These results clearly demonstrated that the CdS component in the nanocomposites was formed into a pure hexagonal phase with high crystallinity. For 0.5 wt% CdS/BNNSs, no obvious characteristic diffraction peaks for BNNSs were observed because of the low amount of BNNSs. It can be seen that all the characteristic peaks of CdS and BNNSs without new peaks in the 10 wt% CdS/BNNSs nanocomposites, indicating there was no new phase produced in the preparation process.

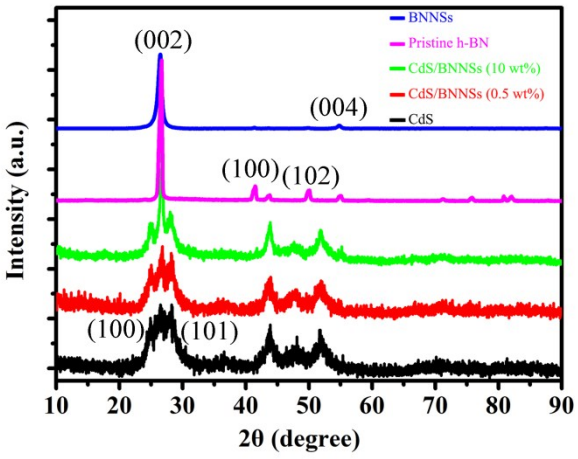

Fig. 4 X-ray diffraction patterns of the as-obtained products. The images from up to bottom are BNNSs, pristine h-BN, CdS/BNNSs nanocomposites (10 wt%), CdS/BNNSs (0.5 wt%) and CdS nanoparticles.

The characterizations of the as-obtained products were also investigated by FTIR and Raman spectra. All the spectra results further confirm the coexistence of BNNSs and CdS in the nanocomposites, which are consistent with the above results (see Supplementary Information S1 and S2).

3.2 Photocatalytic H_2 evolution

BNNSs exhibited an excellent influence on the photocatalytic activity (Figure 5). Fig. 5a shows the rates of H_2 evolution on CdS/BNNSs nanocomposites with different amounts of BNNSs. Even with a small amount of BNNSs, the H_2 evolution rate was noticeably increased. As shown in this image, no H_2 was evolved when BNNSs alone were used as the catalyst, suggesting that BNNSs were inactive for photocatalytic H_2 evolution. CdS nanoparticles alone showed activity for photocatalytic H_2 evolution, but compared with other compositions, the activity was low (188.2 μmol h^{-1} g^{-1}, quantum efficiency of 0.30 % at 420 nm). In the presence of a small amount of BNNSs (0.1 wt%), the rate of H_2 evolution on CdS/BNNSs was increased to 297.9 μmol h^{-1} g^{-1}, perhaps because the amount of BNNSs was not large enough to efficiently load all the CdS nanoparticles. With the increase of the amount of BNNSs in nanocomposites, the rate of H_2 evolution on CdS/BNNSs was further increased and achieved the maximum when the amount of BNNSs was 0.5 wt%. The rate of H_2 evolution on CdS/BNNSs at the optimum adding was 2.3 times higher than that on CdS nanoparticles alone. The corresponding H_2 evolution rate reached 439.4 μmol h^{-1} g^{-1} with apparent quantum efficiency of 0.73% at 420 nm. Further adding of BNNSs in the nanocomposites led to a decrease in the photocatalytic H_2 evolution. In particular, at the BNNSs amount of 1.5 wt%, the photocatalytic activity of CdS/BNNSs nanocomposites decreased to 155.5 μmol h^{-1} g^{-1}. Excess loading of BNNSs could considerably block the absorption of the incident light by CdS, and recombination centers may be introduced at high loadings, which was another factor leads to the decreased activity.[41] As a consequence, a suitable content of BNNSs is crucial for optimizing the photocatalytic activity of CdS/BNNSs nanocomposites.

To investigate the stability of CdS/BNNSs nanocomposites, photocatalytic reaction was carried out for repeated several cycles. The reaction system was evacuated every 5 h. As is shown in Fig. 5b, the rate of H_2 evolution on CdS/BNNSs nanocomposites decreased slightly with every reaction cycle. Therefore, the photocorrosion of CdS during the photocatalytic reactions was supposed to be the main reason for the decreased activity with reaction time, which has been pointed to be a major problem for metal sulfide photocatalysts.[42]

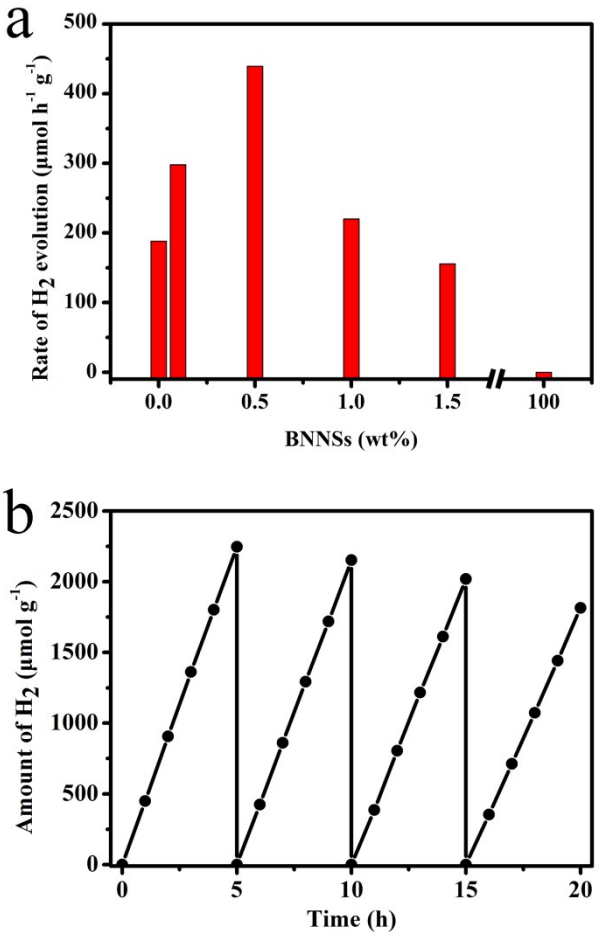

Fig. 5 H_2 evolution reaction results of the as-prepared products. a) Rate of H_2 evolution on CdS/BNNSs nanocomposites. b) H_2 evolution of 0.5 wt% CdS/BNNSs nanocomposites during the photocatalytic stability study. Photocatalytic reaction conditions: 50 mg of the nanocomposites, 100 mL of aqueous solution containing 0.7564 g Na_2S and 4.8036 g Na_2SO_3 and 300 W Xe lamp.

For further study the photocatalytic performance of the CdS/BNNSs nanocomposites, the products which were loaded by Pt were also tested. As shown in Fig. 6, the as-obtained pure CdS, 0.5 wt% CdS/BNNSs nanocomposites was loaded by 0.5% Pt. It can be found that the rates of H_2 evolution became much higher when Pt was loaded, mainly due to the excellent electrical conduction performance of noble metal. Moreover, it was clearly seen that the evolution rate of Pt/CdS/BNNSs still kept much higher than the rate of Pt/CdS, which was consistent with the above results. The rate of Pt/CdS/BNNSs was 5.961 mmol h^{-1} g^{-1} and corresponds to an apparent quantum efficiency of 9.30% (λ_{ex} = 420 nm). In this regard, the photocatalytic activity of the nanocomposites was significantly greater than CdS nanoparticles. Although the results showed a relative lower upside potential than other CdS decorated two-dimension nanosheets such as graphene and MoS_2 nanosheets,[43-44] as a supporter BNNSs really improve the photocatalytic properties of CdS to a large extent.

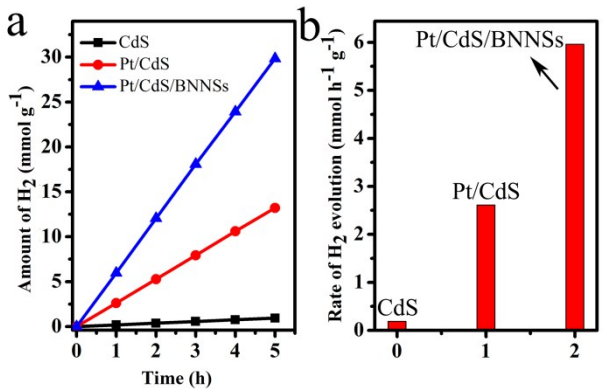

Fig. 6 H_2 evolution reaction results of the as-prepared products. Photocatalytic reaction conditions: 50 mg of the nanocomposites, 100 mL of aqueous solution containing 0.7564 g Na_2S and 4.8036 g Na_2SO_3 and 300 W Xe lamp.

The electrochemical experiments were also conducted to further investigate the separation of photogenerated charge carriers. The photocurrent is mainly determined by the electron–hole pair separation efficiency within the photoelectrodes. As shown in Fig. 7, the transient photocurrent responses of pure CdS nanoparticles and the as-obtained 0.5 wt% CdS/BNNSs nanocomposites were recorded for several on–off cycles of irradiation. Compared with CdS nanoparticles, the CdS/BNNSs nanocomposites exhibited enhanced photocurrent response, which indicated that the number of photo-generated electrons was greatly increased because of coupling with BNNSs nanosheets. Electrochemical impedance spectroscopy (EIS) measurements were adopted to investigate charge transfer and recombination processes at solid/electrolyte interfaces. The diameters of the arc radius on the EIS Nyquist plot of the as-obtained products were shown in Fig. 7b. Smaller diameter implies an effective separation of the photogenerated electron–hole pairs and fast interface charge transfer. It is obvious that the CdS/BNNSs nanocomposites are superior to the CdS nanoparticles in carrier separation and charge transfer, in consistent with the HER analysis.

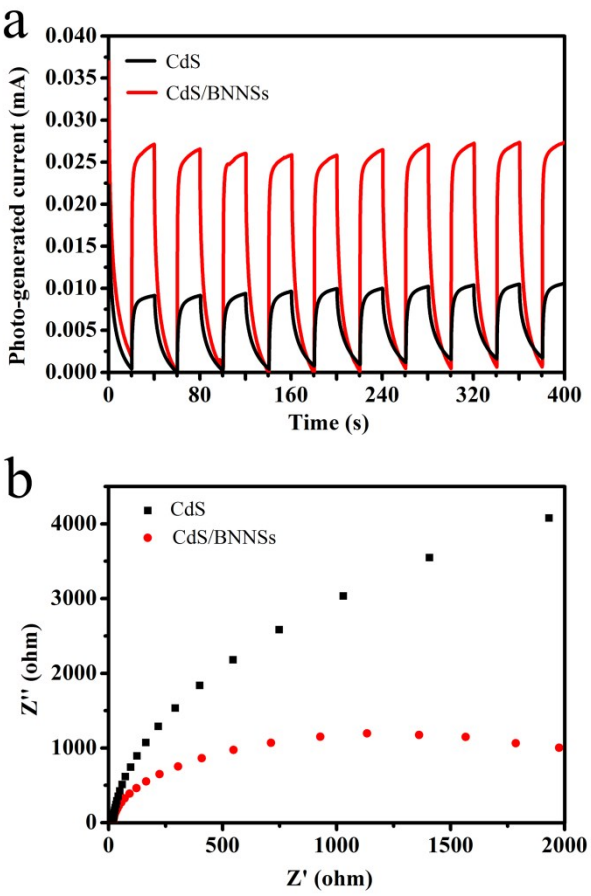

Fig. 7 Transient photocurrent responses (a) and Nyquist impedance plots (b) of pure CdS nanoparticles and CdS/BNNSs nanocomposites.

3.3 The mechanism for the photocatalytic H_2 evolution.

Based on the above results, the proposed mechanism for photocatalytic H_2 production on CdS/BNNSs nanocomposites is shown in Fig. 8. As shown in the schematic representation, CdS nanoparticles are grown on the imperfections and edges of BNNSs. On one hand, due to the characteristics of two-dimensional structure, the nanocomposites can offer a lager specific surface area. More active adsorption sites and photocatalytic reaction centers are provided in this case.[45] On the other hand, CdS nanoparticles and BNNSs are connected with each other by chemical bonds, and the novel nanocomposites broaden the photo absorption region of CdS (see Supplementary Information S5). Under photoexcitation, electron and hole pairs are produced in the conduction band (CB) and valence band (VB) of CdS, and there are still photo electrons generated on the BNNSs surface especially at the imperfections and edges. It is believed that an electronic communication between BNNSs and CdS comes true. The effective electron transport between BNNSs and CdS leads to the enhancement of photocatalytic H_2 evolution. The photogenerated holes are consumed by the sacrificing agents. The electrons will transfer to the connected points and surface of CdS to reduce protons to H_2. So the broad photo absorption region and effective electron transport make the enhancement of photocatalytic H_2 evolution come true.

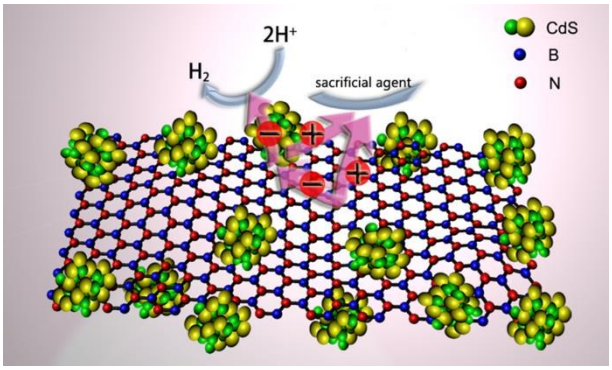

Fig. 8 Schematic illustration of charge separation and transfer in the CdS/BNNSs nanocomposites.

4. Conclusions

Unprecedentedly, the nanocomposites of CdS nanoparticles and BNNSs were designed and fabricated successfully, and the excellent performance of CdS/BNNSs nanocomposites was proved in the field of hydrogen production from water. The in-situ growth method was conducted to prepare CdS/BNNSs nanocomposites which linked together by chemical bonds. The photocatalytic performance of the nanocomposites was studied comparing with pure CdS nanoparticles, and the results showed that BNNSs played an important role in improving the photocatalytic performance. Under optimum conditions, the rate of H_2 evolution can be increased by up to 2.3 times when CdS was loaded with only 0.5 wt% BNNSs and reached 439.4 μmol h^{-1} g^{-1}. It is supposed that when BNNSs are introduced, the broad spectral response and effective electron transport make the enhancement of photocatalytic H_2 evolution come true. This work suggests that the BNNSs supporters can be appealing candidates for the fabrication of various types of BNNSs-based nanocomposites, which will have wide application in the fields of catalysis, environment and new energy materials.

Acknowledgements

This work is supported by the National Natural Science Foundation of China (Contract No. 51321091) and the Fundamental Research Funds of Shandong University.

Notes and references

†Electronic Supplementary Information (ESI) available: See DOI: 10.1039/b000000x/

1 K. S. Novoselov, A. K. Geim, S. V. Morozov, D. Jiang, Y. Zhang, S. V. Dubonos, I. V. Grigorieva and A. A. Firsov, *Science*, 2004, **306**, 666–669.
2 Y. Zhu, S. Murali, W. Cai, X. Li, J.W. Suk, J. R. Potts and R. S. Ruoff, *Adv. Mater.*, 2010, **22**, 3906–3924.
3 K. R. Paton, *Nat. Mater.*, 2014, **13**, 624–630.
4 P. Thangasamy and M. Sathish, *CrystEngComm*, 2015, **17**, 5895–5899.
5 K. Zhou, N. Mao, H. Wang, Y. Peng and H. Zhang, *Angew. Chem. Int. Ed.*, 2011, **50**, 10839–10842.
6 S. Z. Butler, S. M. Hollen, L. Cao, Y. Cui, J. A. Gupta, H. R. Gutie´rrez, T. F. Heinz, S. S. Hong, J. Huang, A. F. Ismach, E. J. Halperin, M. Kuno, V. V. Plashnitsa, R. D. Robinson, R. S. Ruoff, S. Salahuddin, J. Shan, L. Shi, M. G. Spencer, M. Terrones, W. Windl and J. E. Goldberger, *ACS Nano,* 2013, **7**, 2898–2926.
7 Q Li, G Zhang, F Liu, K Han, M. R. Gadinski, C Xiong and Q. Wang, *Energy Environ. Sci.*, 2015, **8**, 922–931.
8 Amet, F. Williams, J. R. Garcia, A. G. F. Yankowitz, M. Watanabe, K. Taniguchi and T. Goldhaber-Gordon, *Phys. Rev. B*, 2012, **85** (7), 073405.
9 T. L. Li and S. L. Hsu, *J. Phys. Chem. B*, 2010, **114** (20), 6825–6829.
10 H. Yan, Y. Tang, J. Su and X. Yang, *Appl. Phys. A*, 2014, **114**, 331–337.
11 C. Huang, C. Chen, X. Ye, W. Ye, J. Hu, C. Xu and X. Qiu, *J. Mater. Chem. A*, 2013, **1**, 12192–12197.
12 M. Gao, A. Lyalin and T. Taketsugu, *J. Phys. Chem. C*, 2012, **116** (16), 9054–9062.
13 H. J. Zhao, J.Z. Song, X. F. Song, Z. Yan and H. B. Zeng, *J. Mater. Chem. A*, 2015, **3**, 6679–6684.
14 M. Bernardi, M. Palummo and Jeffrey C. Grossman, *Phys. Rev. Lett.*, 2012, **108**, 226805.
15 G. Brasse, S. Maine, A. Pierret, P. Jaffrennou, B. A. T. Tout, F. Ducastelle and A. Loiseau, *Phys. Status Solidi B*, 2010, **247**, 3076–3079.
16 H. Zeng, C. Zhi, Z. Zhang, X. Wei, X. Wang, W. Guo, Y. Bando and D. Golberg, *Nano. Lett.*, 2010, **10**, 5049–5055.
17 V. Nicolosi, M. Chhowalla, M. G. Kanatzidis, M. S. Strano and J. N. Coleman, *Science*, 2013, **340**, 6139.
18 Y. S. Perets, L. Yu. Matzui, L. L. Vovchenko, Yu. I. Prylutskyy, P. Scharff and U. Ritter, *J. Mater. Sci.*, 2014, **49**, 2098–2105.
19 L. F. He, J. Shirahata, H. Suematsu, T. Nakayama, T. Suzuki, W. Jiang and K. Niihara, *Materials Letters*, 2014, **117**, 120–123.
20 Z. Lina, A. Mcnamara, Y. Liu, K. S. Moon and C. P. Wong, *Compos. Sci. Technol.*, 2014, **90**, 123–128.
21 K. Uosaki, G. Elumalai, H. Noguchi, T. Masuda, A. Lyalin, A. Nakayama and T. Taketsugu, *J. Am. Chem. Soc.*, 2014, **136**, 6542–6545.
22 V. L. Solozhenko, A. G. Lazarenkob, J. P. Petitet and A. V. Kanaev, *J. Phys. Chem. Solids*, 2001, **62**, 1331–1334.
23 D. Golberg, Y. Bando, Y. Huang, T. Terao, M. Mitome, C. Tang and C. Zhi, *ACS Nano*, 2010, **4**, 2979–2993.
24 S. Azevedo, J. R. Kaschny, C. M. C. D. Castilho and F. D. B. Mota, *Eur. Phys. J. B*, 2009, **67**, 507–512.
25 L. Britnell, R. V. Gorbachev, R. Jalil, B. D. Belle, F. Schedin, M. I. Katsnelson, L. Eaves, S. V. Morozov, A. S. Mayorov, N. M. R. Peres, A. H. C. Neto, J. Leist, A. K. Geim, L. A. Ponomarenko and K. S. Novoselov, *Nano Lett.*, 2012, **12**, 1707–1710.
26 Y. Li, L. Tang, S Peng, Z Lia and G. Lu, *CrystEngComm*, 2012, **14**, 6974–6982.
27 N. Bao, L. Shen, T. Takata and K. Domen, *Chem. Mater.*, 2008, **20**, 110–117.
28 J. Xu, L. Wang and X. Cao, *Chem. Eng. J.,* 2016, **283**, 816–825.
29 P. V. Kamat, *J. Phys. Chem. C*, 2007, **111**, 2834–2860.

30 X. Wang, B. Yuan, Z. Xie, D. Wang and R. Zhang, *J. Colloid Interf. Sci.*, 2015, **446**, 150–154.

31 J. J. Zhou, R. Wang, X. L. Liu, F. M. Peng, C. H. Li, F. Teng and Y. P. Yuan, *Appl. Surf. Sci*, 2015, **346**, 278–283.

32 J. S. Jie, W. J. Zhang, Y. Jiang, X. M. Meng, Y. Q. Li and S. T. Lee, *Nano Lett.* 2006, **6** (9), 1887–1892.

33 S. Chen, X. Chen, Q. Jiang, J. Yuan, C. Lin and W. Shangguan, *Appl. Surf. Sci*, 2014, **316**, 590–594.

34 J. N. Coleman, M. Lotya, A. O'Neill, S. D. Bergin, P. J. King, U. Khan, K. Young, A. Gaucher, S. De, R. J. Smith, I. V. Shvets, S. K. Arora, G. Stanton, H.Y. Kim, K. Lee, G. T. Kim, G. S. Duesberg, T. Hallam, J. J. Boland, J. J. Wang, J. F. Donegan, J. C. Grunlan, G. Moriarty, A. Shmeliov, R. J. Nicholls, J. M. Perkins, E. M. Grieveson, K. Theuwissen, D. W. McComb, P. D. Nellist and V. Nicolosi, *Science*, 2011, **331**, 568–571.

35 Kenneth A. Jackson, *Kinetic Processes*, WILEY–VCH Verlag Gmbh, 2004, pp. 191.

36 L. Ci, L. Song, C. Jin, D. Jariwala, D. Wu, Y. Li, A. Srivastava, Z. F.Wang, K. Storr, L. Balicas, F. Liu and P. M. Ajayan, *Nature Materials*, 2010, **9**, 430–435.

37 Y. Shi, C. Hamsen, X. Jia, K. K. Kim, A. Reina, M. Hofmann, A. L. Hsu, K. Zhang, H. Li, Z. Y. Juang, M. S. Dresselhaus, L. J. Li and J. Kong, *Nano Lett.*, 2010, **10**, 4134–4139.

38 J. Wang, S. Liang, L. Ma, S. Ding, X. Yu, L. Zhou and Q. Wang, *CrystEngComm*, 2014, **16**, 399–405.

39 T. Jia, A. Kolpin, C. Ma, R. C. Chan, W. M. Kwokc and S. C. E. Tsang, *Chem. Commun.*, 2014, **50**, 1185–1188.

40 M. Du, Y. Wu, X. Hao, *CrystEngComm*, 2013, **15**, 1782–1786.

41 X. Zong, J. Han, G. Ma, H. Yan, G. Wu and C. Li, *J. Phys. Chem. C*, 2011, **115**, 12202–12208.

42 J. Chen, X. Wu, L. Yin, B. Li, X. Hong, Z. Fan, B. Chen, C. Xue and H. Zhang, *Angew. Chem. Int. Ed.*, 2015, **54**, 1210–1214; *Angew. Chem.*, 2015, **127**, 1226–1230.

43 Q Li, B Guo, J. Yu, J. Ran, B. Zhang, H. Yan and J. R. Gong, *J. Am. Chem. Soc.,* 2011, **133**, 10878–10884.

44 K. Chang , M. Li , T. Wang, S. Ouyang, P. Li, L. Liu and J. Ye, *Adv. Energy Mater*. **2015**, 1402279.

45 Q. Li, X. Li, S. Wageh, A. A. Al-Ghamdi and J. Yu, *Adv. Energy Mater*. 2015, **5**, 1500010.

A table of contents entry

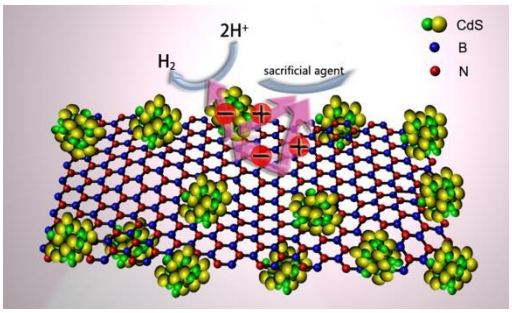

A high efficiency of the photocatalytic H_2 production was achieved using BNNSs decorated with CdS as photocatalysts.